Journal of Alloys and Compounds 509 (2011) 2256–2262

Contents lists available at ScienceDirect

Journal of Alloys and Compounds

journal homepage: www.elsevier.com/locate/jallcom

Microstructural study of Ag_2S doped silver molybdate glass-nanocomposites

B. Deb, A. Ghosh*

Department of Solid State Physics, Indian Association for the Cultivation of Science, Jadavpur, Kolkata 700032, India

ARTICLE INFO

Article history:
Received 12 August 2010
Received in revised form 28 October 2010
Accepted 28 October 2010
Available online 10 November 2010

Keywords:
Glass-nanocomposites
Microstructure
IR spectra

ABSTRACT

Glass-nanocomposites in the system Ag_2S–Ag_2O–MoO_3 have been synthesized by quenching of melts. Microstructural studies of the samples have been accomplished using X-ray diffraction, high-resolution transmission electron microscopy and field emission scanning electron microscopy. The formation of glass-nanocomposites and the presence of different crystalline phases, namely α-Ag_2MoO_4, $Ag_2Mo_2O_7$ and γ-Ag_2S dispersed throughout in the glassy matrix have been confirmed from these studies. The formation and growth of different nanocrystalline phases have been studied as a function of composition and heat-treatment time. The effects of variation of Ag_2S content and heat-treatment on the local network structure within the glassy matrix have been explored using FT-IR spectroscopic study.

1. Introduction

Glass-nanocomposites are produced when crystallite particles of nanometer dimension are dispersed within the host glass matrix [1]. These forms of glasses and glass-nanocomposites have been attracting much interest because of their excellent adjustability of compositions, microstructures and technological applications [2–5]. The crystallization in glasses and glasses-nanocomposites and their other properties have been investigated by several techniques such as optical, thermal, ion-exchange process, etc. [6–8]. The heat-treatment induced crystallization in glasses depends on various factors such as defect state, structure, composition, free energy and also on interfacial energy between the embedded crystallites and the glass matrix [9]. The formation of glasses and glass-nanocomposites with different glass formers such as B_2O_3, P_2O_5, TeO_2, etc. and transition metal oxides like V_2O_5 have been reported [10–12]. The variation of the microhardness properties and the ionic conductivity due to nanocrystallization in a few silver borate glasses with the addition of hard ceramic powders has been reported [10], where a decrease of the conductivity in glass-nanocomposites in comparison with the parent glass matrix has been observed. It has been reported [13] that the thermal treatment of the silver vanadate glasses near the glass transition temperature leads to the enhancement of the conductivity, whereas the annealing of these glasses at much higher temperatures leads to nanocrystallization, which decreases the conductivity due to the change of the interfacial regions and defect states. The precipitation of nanoparticles within the glassy matrix can thus either enhance or reduce the conductivity. To tailor the properties of these nanocomposites and to make them suitable for practical application, the understanding of their microsructural aspect is foremost important [14,15].

Among the various transition metal-oxides, molybdenum trioxide (MoO_3) has attracted much interest because of its multifaceted functional properties like applications as a catalyst in selective oxidation reaction, information display systems, sensors, photochromic, and electrochromic systems. Although structural studies on different tellurite and phosphate glasses have been recently reported [16,17], the investigation of molybdate glass systems has not gained much attention [18]. A few studies on the silver ion conducting molybdate glasses [19] and glass-nanocomposites with dispersed nanocrystalline phases have been reported [20]. It has been observed that the formation of these nanocrsytallites gives rise to different characteristics [20] from those of the host glass matrix, such as the electrical conductivity, which decreases with the increase of the size of the nanoparticles [20]. In a few AgI doped silver molybdate glasses, the formation of superionic α-AgI phase [21] frozen in the glass matrix has been observed which drastically enhances the conductivity. The NMR studies of the silver-molybdate glasses [22] show a strong dependence of stability of the glass network on the MoO_3 content. It has been observed that the stability of the network is higher for the low MoO_3 content, whereas at higher MoO_3 content the system is more prone to crystallization due to formation of MoO_6 clusters. However, only a few studies on the glass-nanocomposites containing Ag_2S have been reported [23].

In the present work, we have reported the synthesis and microstructure of silver molybdate glass-nanocomposites containing Ag_2S, in which nanosize particles are dispersed within the glass matrix. The influence of the thermal treatment on the growth of the

* Corresponding author. Tel.: +91 3324734971; fax: +91 3324732805.
E-mail address: sspag@iacs.res.in (A. Ghosh).

0925-8388/$ – see front matter © 2010 Elsevier B.V. All rights reserved.
doi:10.1016/j.jallcom.2010.10.197

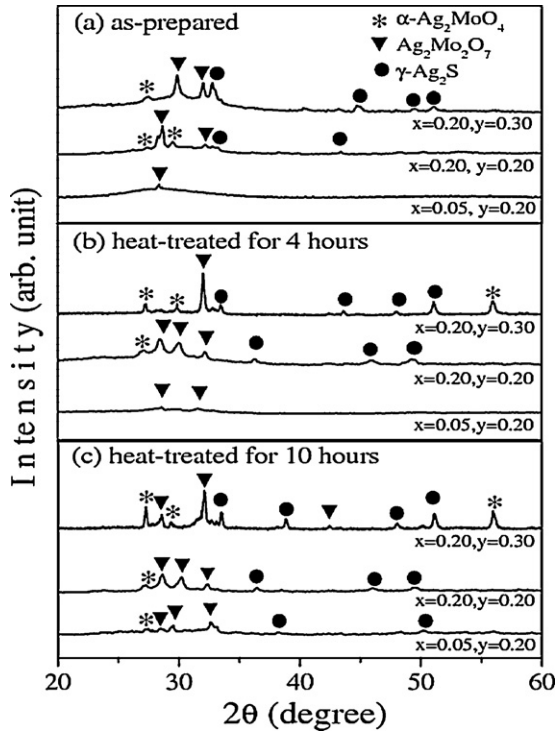

Fig. 1. X-ray diffraction patterns of some as-prepared and heat-treated samples of compositions xAg$_2$S–$(1-x)(y$Ag$_2$O–$(1-y)$MoO$_3$).

nanoparticles in host glass matrix has been efficiently investigated in order to understand the exotic features of nanocrystalline materials. The influence of Ag_2S content on the as-prepared as well as on the heat-treated glasses has been also investigated. It has been observed that the formation of nanocrsytallites is less for the compositions with low Ag_2S content, whereas the crystallization of the compositions with high Ag_2S content is significant.

2. Experimental procedures

Glass samples of compositions xAg$_2$S–$(1-x)(y$Ag$_2$O–$(1-y)$MoO$_3$) where $x = 0.05$, 0.10, 0.15, 0.20 and $y = 0.20$ and 0.30 were synthesized by conventional melt quenching technique. The appropriate mixtures of Ag_2S, $AgNO_3$ and MoO_3 were heated initially in alumina crucibles in an electric furnace at 450 °C for 4 h for denitrogenation of $AgNO_3$. Then the mixtures were melted in the temperature range of 850–950 °C depending on composition and equilibrated for 2 h. The melts were then quenched by pressing them between two aluminum plates. All the as-prepared samples were heat-treated for 4, 6 and 10 h above the glass transition temperature. The X-ray diffraction patterns of the as-prepared and the heat-treated samples were recorded in a X-ray diffractometer (Bruker, model D8 Advanced AXS) using Cu Kα radiation (wavelength = 1.54 Å) at a scan speed of 0.02°/s. For scanning electron microscopic (SEM) studies, the samples were mounted on a specimen stub and platinum was sputtered on the samples under vacuum. The SEM micrographs were then taken in a field-emission scanning electron microscopy (JEOL, model JSM-6700F). For transmission electron microscopic (TEM) studies, a few mg of powder samples were sonicated in distilled water for 15 min in an ultrasonic bath (EYELA) and then a few drops of the sonicated solution were dropped in a 300 mesh carbon coated copper grid. The TEM micrographs of the samples were taken in a transmission electron microscope equipped with high-resolution facility (JEOL, model JEM-2010). The Fourier transform infrared (FTIR) spectra of the powder samples in KBr matrix in the ratio 1:100 were recorded in a FTIR spectrometer (SHIMADZU, model FTIR-8400S).

3. Results and discussion

The X-ray diffraction (XRD) patterns for some as-prepared and heat-treated samples of compositions xAg$_2$S–$(1-x)(y$Ag$_2$O–$(1-y)$MoO$_3$) are shown in Fig. 1. It is observed that for the as-prepared samples, different crystalline peaks are present, in addition to broad haloes, indicating the existence of crystalline phases embedded in the glassy matrix. The interplaner spacing (d values) of these crystallites was calculated using Bragg's law and the corresponding crystalline phases and ($h\,k\,l$) planes were identified by comparing the d-values with those from ICDD datasheet [24]. The presence of $Ag_2Mo_2O_7$ crystallites has been identified in the as-prepared compositions having 0.05 and 0.10 mole fraction of Ag_2S for fixed 0.20 mole fraction of Ag_2O and for 0.05 mole fraction of Ag_2S for fixed Ag_2O content of 0.30 mole fraction. The presence of crystalline phases of α-Ag_2MoO_4, $Ag_2Mo_2O_7$ and γ-Ag_2S crystallites has been observed in the as-prepared samples with Ag_2S content of 0.15 and 0.20 mole fraction. The heat-treatment for 4 h for the sample $x = 0.05$ with Ag_2O content of 0.20 mole fraction provides additional peaks corresponding to $Ag_2Mo_2O_7$ crystalline phase along with the peaks observed in the as-prepared sample. The samples with higher Ag_2S content of 0.10, 0.15 and 0.20 mole fraction, when heat-treated for 4 h, shows considerable increase in the crystalline phase of α-Ag_2MoO_4, $Ag_2Mo_2O_7$ and γ-Ag_2S crystallites. After heat-treatment for 10 h the samples having 0.05 and 0.20 mole fraction Ag_2S leads to the appearance of several additional peaks corresponding to the crystalline phase of α-Ag_2MoO_4, $Ag_2Mo_2O_7$ and γ-Ag_2S crystallites. It is observed that on heat treatment the broad-hump decreases with the appearance of several crystalline peaks indicating that heat-treatment increases the crystallinity within the glassy matrix.

The average size of the crystallites has been estimated using Debye–Scherrer formula [25], given by

$$D = \frac{0.9\lambda}{(\beta \cos\theta)}, \quad (1)$$

where D denotes the average crystal size, λ is the wavelength of X-ray, β is the full width at half maximum (in radians) and θ is the corresponding Bragg angle. The variation of the average size of the crystallites with Ag_2S content is shown in Fig. 2, which indicates nanocrystalline nature of the crystallites. It is observed that there is a slight increasing tendency of the average particle size with increasing Ag_2S content. It is also noted that the average particle size increases appreciably for the samples heat-treated for 4 h

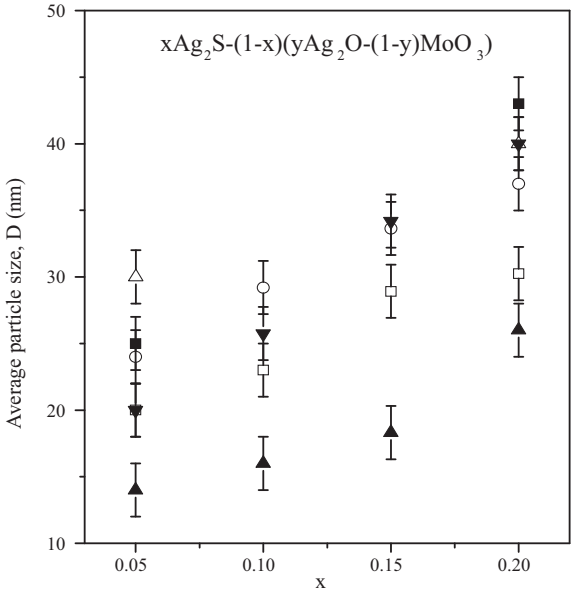

Fig. 2. Composition dependence of the average particle size, D of the compositions xAg$_2$S–$(1-x)(y$Ag$_2$O–$(1-y)$MoO$_3$): □ for the as-prepared samples $y = 0.20$; ○ for the samples $y = 0.20$ heat-treated for 4 h; △ for the samples $y = 0.20$ heat-treated for 10 h; ▲ for the as-prepared samples $y = 0.30$; ▼ for the samples $y = 0.30$ heat-treated for 4 h and ■ for the samples $y = 0.30$ heat-treated for 10 h.

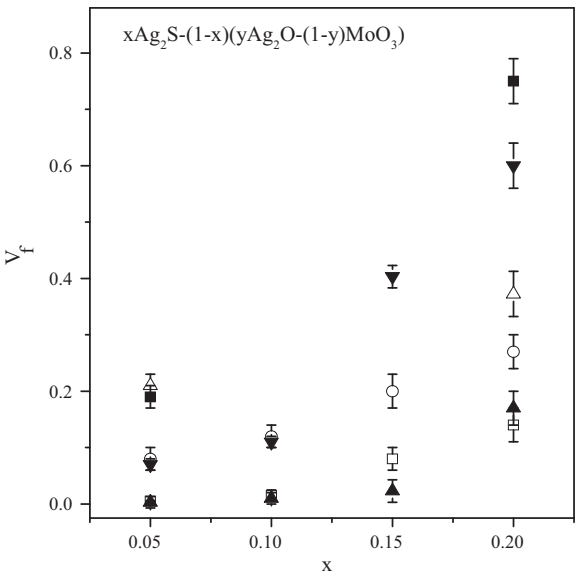

Fig. 3. Variation of crystalline volume fraction (V_f) with Ag_2S content for the as-prepared and heat-treated samples of compositions xAg_2S–$(1-x)(yAg_2O$–$(1-y)MoO_3)$: □ for the as-prepared samples $y = 0.20$; ○ for the samples $y = 0.20$ heat-treated for 4 h; Δ for the samples $y = 0.20$ heat-treated for 10 h; ▲ for the as-prepared samples $y = 0.30$; ▼ for the samples $y = 0.30$ heat-treated for 4 h and ■ for the samples $y = 0.30$ heat-treated for 10 h.

compared to as-prepared samples, whereas heat-treatment for 10 h increases the average particle size only slightly larger in comparison to the samples heat-treated for 4 h. The formation and growth of multiphase nanocrystallites makes it difficult to precisely identify the true origin of growth of nanocrystallites caused by thermal treatment. However, the surface nucleation or a combination of surface and internal nucleation can influence the nucleation and growth behavior in these glass-nanocomposites, as revealed from the TEM and SEM studies discussed later.

To understand qualitatively the crystallization tendency of the as-prepared samples, the crystalline volume fraction has been calculated from the X-ray diffraction data, using the following relation [26]

$$V_f = \frac{A_c}{(A_c + A_a)}, \quad (2)$$

where V_f is the volume fraction of nanocrystallites, A_c and A_a are the total integrated areas corresponding to the crystalline and amorphous phases, respectively. The integrated areas corresponding to amorphous and crystalline phases have been separated by the deconvolution of the amorphous haloes and the crystalline peaks. The crystalline volume fraction V_f obtained in this way is shown in Fig. 3 as a function of Ag_2S content for all the as-prepared and heat-treated compositions. It is observed that the crystalline volume fraction is very low (<0.10) for the as-prepared samples with 0.05, 0.10 and 0.15 mole fraction of Ag_2S content for fixed Ag_2O content of 0.20 and 0.30 mole fraction. However, the crystalline volume fraction is much higher for the samples with high Ag_2S content having 0.20 mole fraction. The crystallinity increases drastically for samples heat-treated for 4 and 10 h. It is observed that the crystalline volume fraction exceeds 0.75 for duration of heat-treatment for 10 h for the sample with highest Ag_2S content of 0.20 mole fractions for Ag_2O content of 0.30 mole fraction and around 0.40 for samples with 0.20 mole fraction of Ag_2O content. Thus the dominating effect of prolonged heat-treatment is to increase the fraction of crystalline phases rather than to increase the size of the crystallites.

Fig. 4 shows the TEM images for some as-prepared and heat-treated samples, while the insets show the corresponding selected area electron diffraction (SAED) patterns. The formation of nanoparticles is evident from the images for all the samples. The average particle sizes estimated from these micrographs are listed in Table 1 and are close to that obtained from XRD. The SAED patterns show sharp bright spots along with characteristic amorphous rings for the as-prepared samples. From the diffraction spot in the SAED patterns, the interplaner distances (d values) have been calculated and the different crystalline phases have been obtained by comparing them with those given in ICDD datasheet [24]. The characteristic amorphous rings of the SAED pattern get diminished for the heat-treated samples, clearly depicting the increase of crystalline order as observed for the heat-treated samples [Fig. 4(c)–(e)] compared to as-prepared samples [Fig. 4(a) and (b)]. The lattice fringe patterns are clearly observed in the high-resolution image [Fig. 4(f)] for a particular crystallite [Fig. 4(e)]. The interplaner spacing (d) has been calculated from these fringe patterns as indicated in the figure. The fast Fourier transform (FFT) of the corresponding HR-TEM image, shown in the inset in Fig. 4(f), reveals the hexagonal structure of the corresponding crystallite. A rod like growth of the matrix having embedded nanoparticles on its surfaces is noticed for the samples with 0.20 mole fraction of Ag_2S content, heat-treated for 10 h. The heat-treatment thus considerably increases the degree of crystallization, accompanied by formation of different crystalline phases. This result indicates that on prolonged heat-treatment time particle size does not increase much, whereas different new nuclei sites grow so that crystallinity increases.

To study the distribution of nanoparticles within the matrix, we have obtained histograms of particles count as a function of particle

Table 1
Average particle size (D) obtained from XRD, TEM and lognormal distribution for xAg_2S–$(1-x)$ $(yAg_2O$–$(1-y)MoO_3)$ glass-nanocomposites.

Compositions	Average size from XRD (nm) (±2)	Average size from TEM (nm) (±3)	Average size from lognormal distribution (nm) (±2)
$y = 0.20$ As-prepared			
$x = 0.05$	20	22	22
$x = 0.10$	23	25	24
$x = 0.15$	29	27	29
$x = 0.20$	30	25	20
4 h Heat-treated			
$x = 0.05$	24	25	24
$x = 0.10$	29	31	30
$x = 0.15$	34	36	36
$y = 0.20$	37	39	40
10 h Heat-treated			
$x = 0.05$	30	33	31
$x = 0.20$	40	43	43
$y = 0.30$ As-prepared			
$x = 0.05$	14	14	14
$x = 0.10$	16	16	16
$x = 0.15$	18	19	18
$y = 0.20$	26	27	27
4 h Heat-treated			
$x = 0.05$	20	23	22
$x = 0.10$	26	27	27
$x = 0.15$	34	34	33
$y = 0.20$	40	42	40
10 h Heat-treated			
$x = 0.05$	25	26	27
$y = 0.20$	43	44	44

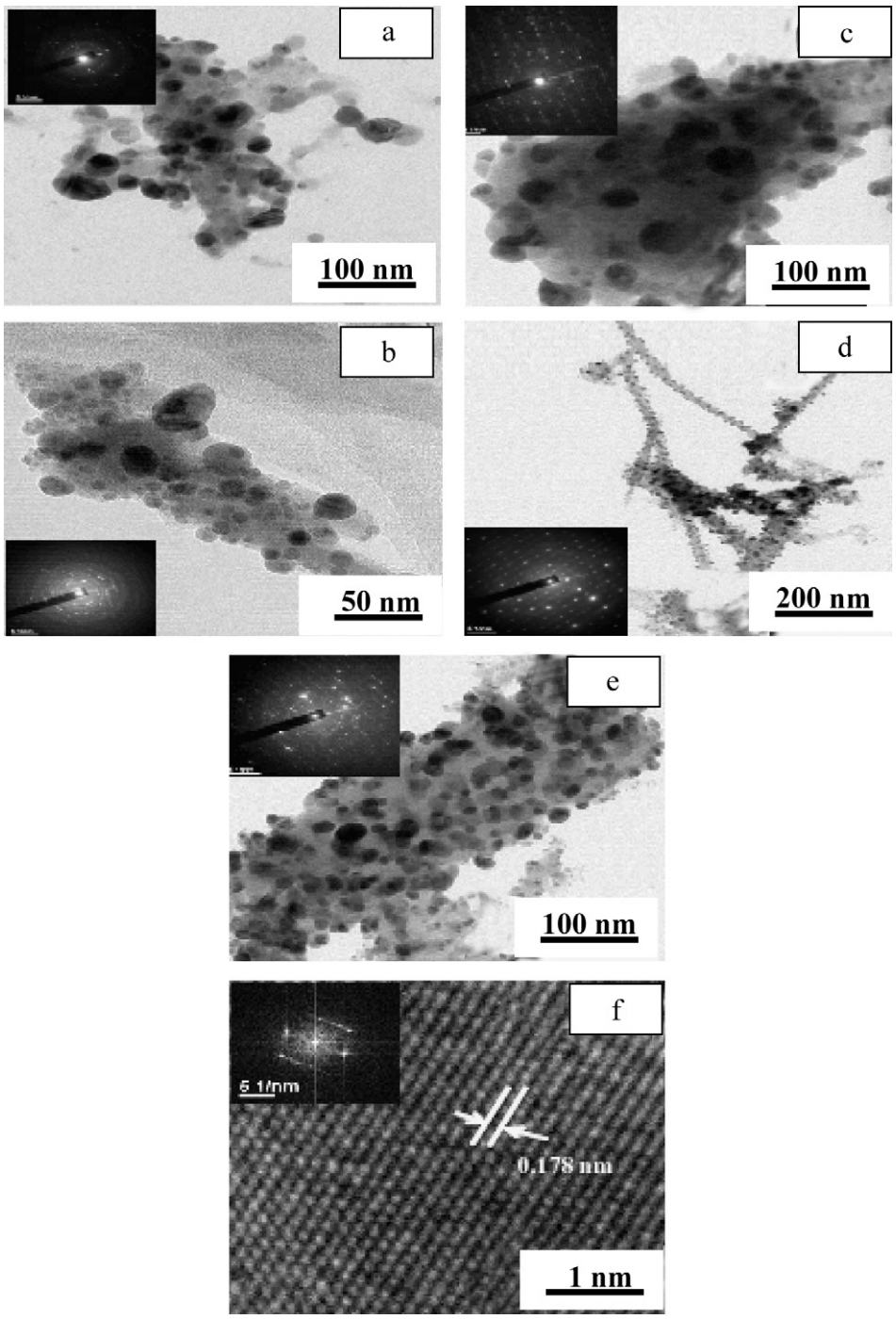

Fig. 4. TEM images for some as-prepared and heat-treated samples of composition xAg_2S–$(1-x)(yAg_2O$–$(1-y)MoO_3)$: (a) for the as-prepared sample $x = 0.20$, $y = 0.20$; (b) for the as-prepared sample $x = 0.20$, $y = 0.30$; (c) for the sample $x = 0.15$, $y = 0.20$ heat-treated for 4 h; (d) for the sample $x = 0.20$, $y = 0.20$ heat-treated for 10 h; (e) for the sample $x = 0.20$, $y = 0.30$ heat-treated for 10 h. The insets in all these figures show the corresponding SAED pattern; (f) HR-TEM image for a particular crystallite of (e), where the inset show the corresponding FFT pattern.

size. Fig. 5 shows the particle histogram of a particular composition. These particle distributions have been fitted to the lognormal distribution function [27] given by the relation

$$f(r) = \left\{\frac{1}{(\ln\sigma\sqrt{(2\pi)})}\right\} \exp\left[\frac{-(\ln r - \ln\rho)}{(2(\ln\sigma)2}\right], \quad (3)$$

where r is particle diameter, ρ is the geometric mean diameter and σ is the dimensionless geometric standard deviation. Approximately 80–100 particles have been sampled from several areas in the TEM images and the particle size has been calculated using a software programme ImageJ. The average particle size obtained from lognormal distribution for different compositions is listed in Table 1. It is noted that the average diameters obtained from the fits are in close agreement with those obtained from the XRD data.

Fig. 6 shows SEM images of several as-prepared and heat-treated samples. The presence of distributed nanoparticles within the glassy matrix is evident from these images. The as-prepared samples [Fig. 6(a) and (b)] clearly reveal the presence of nanoparticles dispersed throughout within the glassy matrix. It may be noted that in the sample heat-treated for 4 h [Fig. 6(c)] the particle sizes are bigger and the agglomeration of particles occurs due to heat-treatment. The micrograph for sample heat-treated for 10 h

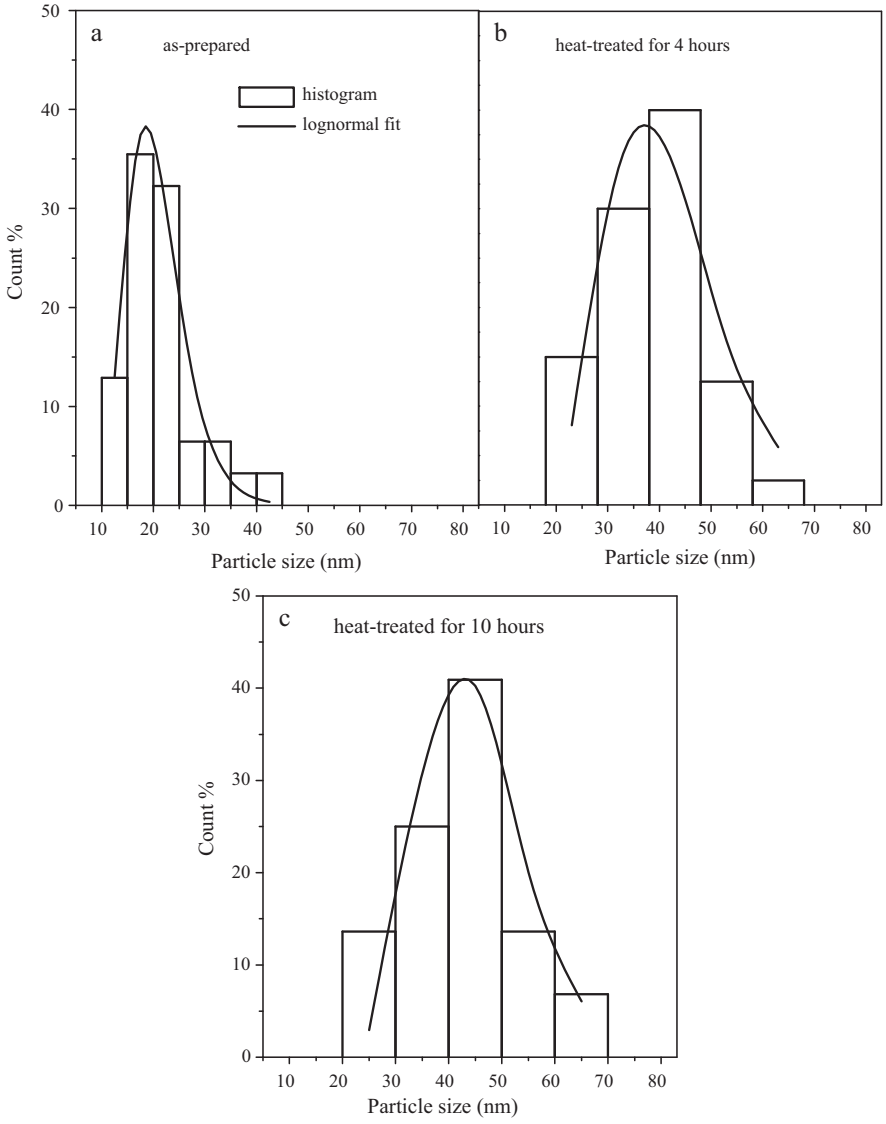

Fig. 5. Histograms for particle distribution shown for as-prepared and heat-treated sample of composition $0.20Ag_2S–0.80(0.20Ag_2O–0.80MoO_3)$. The solid lines are the fits to lognormal distribution [Eq. (3)].

[Fig. 6(d)] clearly shows rod like growth of the glassy matrix with dispersed nanoparticles of slightly larger size. This behavior is similar to that observed from the TEM micrographs.

Fig. 7 shows the FTIR spectra for some as-prepared as well as heat-treated samples. It is observed that for the as-prepared samples shown in Fig. 7(a), two prominent absorption bands around 840 cm^{-1} and 685 cm^{-1} are observed for $y = 0.20$ and absorption band around 480 cm^{-1}, 560 cm^{-1}, 685 cm^{-1}, 840 cm^{-1}, 880 cm^{-1} and 1620 cm^{-1} are observed for samples with Ag_2O content of 0.30 mole fraction. The absorption band at 480 cm^{-1} and 560 cm^{-1} is assigned to the symmetric and asymmetric stretching vibration of Mo–O–Mo bond in $Mo_2O_7^{2-}$ anions respectively [28]. The absorption band at 685 cm^{-1} assigned to the asymmetric vibration of Mo–O–Mo bond of the condensed molybdate anions [29] and the absorption band at around 840 cm^{-1} is attributed to the stretching vibration of MoO_4^{2-} anions [30]. The band at 880 cm^{-1} is assigned to Mo–O–Mo bridge bonds in MoO_6 groups. The band at 1620 cm^{-1} is due to O–H bond of water. It may be noted that the position of the band remains almost unchanged with addition of Ag_2S content. The presence of additional absorption band for samples with 0.30 mole% Ag_2O content compared to that of 0.20 mole fraction of Ag_2O, in turn, indicates that increasing MoO_3 content in the glass composition considerably influences the network structure. The appearance of several additional absorption bands is observed for the samples heat-treated for 4 h indicating the structural modification occurring in the glass matrix due to heat treatment. In comparison to the as-prepared samples with fixed content of 0.20 mole fraction of Ag_2O, the samples heat-treated for 4 h show additional absorption bands at ~570 cm^{-1}, 750 cm^{-1} and 880 cm^{-1}, where the band at 570 cm^{-1} is assigned to the symmetric stretching of Mo–O–Mo bond in $Mo_2O_7^{2-}$ anions and the band at 750 cm^{-1} is attributed to the vibration of tetrahedral orthomolybdate MoO_4^{2-} anion [31]. However, the samples with fixed Ag_2O content of 0.30 mole fraction, when heat-treated for 4 h [Fig. 7(b)], show no additional absorption bands compared to the corresponding as-prepared samples. After heat-treatment for 10 h the samples having 0.05 and 0.20 mole fraction of Ag_2S content for fixed Ag_2O mole fraction of 0.20 show two additional absorption bands at ~460 cm^{-1} and ~700 cm^{-1}, which are assigned to the vibrational modes of Mo-O tetrahedra similar to that existing within the chain structure in crystalline $Na_2Mo_2O_7$ and to Mo (octahedra)–O–Mo (octahedra) similar to the crystalline $K_2Mo_2O_7$, respectively. The samples with 0.05 and 0.20 mole fraction of Ag_2S content for constant Ag_2O mole fraction 0.30, when heat-treated for 10 h, show

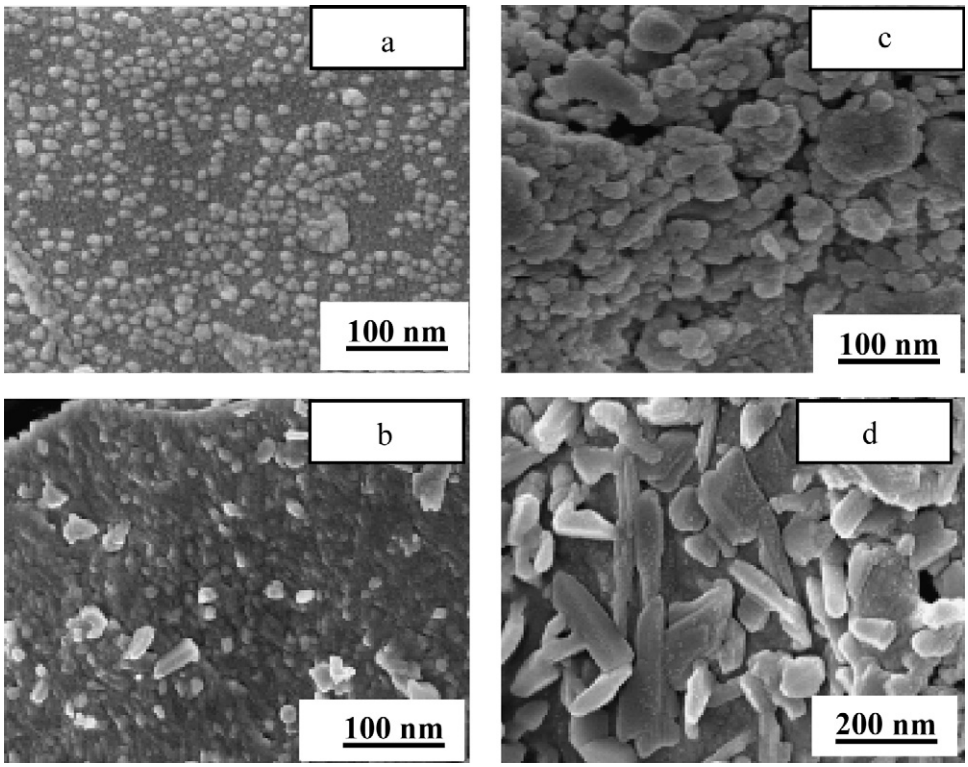

Fig. 6. SEM images for some as-prepared and heat-treated samples of composition $xAg_2S–(1-x)(yAg_2O–(1-y)MoO_3)$: (a) for the as-prepared sample $x = 0 = 0.05$, $y = 0.20$; (b) for the as-prepared sample $x = 0.05$, $y = 0.30$; (c) for the sample $x = 0.05$, $y = 0.30$ heat-treated for 10 h; (d) for the sample $x = 0.20$, $y = 0.30$ heat-treated for 10 h.

one additional absorption band at ~755 cm^{-1} compared to samples heat-treated for 4 h, which is attributed to the vibrational mode of tetrahedral orthomolybdate MoO_4^{2-} anion. The above results indicate that due to heat-treatment the MoO_4^{2-} anions are transformed to more complex structural units such as interlinked MoO_6 octahedral and MoO_4 tetrahedral units.

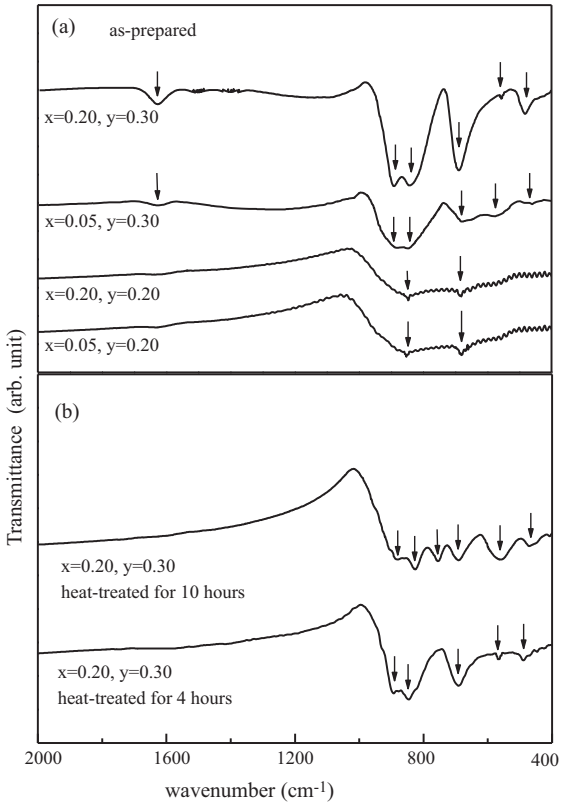

Fig. 7. FTIR spectra of some as-prepared and heat-treated samples of compositions $xAg_2S–(1-x)(yAg_2O–(1-y)MoO_3)$ shown.

4. Conclusions

The synthesis and microstructure of $Ag_2S–Ag_2O–MoO_3$ glass-nanocomposites have been studied using XRD, TEM and SEM. The presence of dispersed different nano-crystalline phases of α-Ag_2MoO_4, $Ag_2Mo_2O_7$ and γ-Ag_2S has been observed in the as-prepared samples. The heat-treatment of the as-prepared samples for short duration of time increases the average particle size of these nanocrystalline phases, accompanied by increase in the crystallinity. The rod like growth of the glassy matrix with dispersed nanoparticles have been observed for prolonged heat-treated samples suggesting that prolonged heat-treatment has predominant effects on increasing the crystallinity rather than increasing the crystallites size. The FTIR spectra reveal that due to heat-treatment modification of the network structure occurs and MoO_4^{2-} anions are transformed into more complex structural units due to the formation and growth of different crystalline phases. The formation and growth of nanocrystallites within the glass-matrix have profound impact on the mechanical, electrical and chemical properties and is under investigation.

Acknowledgements

BD thanks CSIR for providing Research Fellowship (via award no. 09/080(0564)/2007-EMR-I). The authors thankfully acknowledge the financial assistance for the work provided by the Council of Scientific and Industrial Research (CSIR) via grant no. 03 (1095)/07/EMR-II. The support grant by the Department of Science and Technology, Government of India through its Nano Initiative Programme is thankfully acknowledged.

References

[1] P. Knauth, J. Electroceram. 5 (2000) 111–125.
[2] G.S. Murugan, K.B.R. Varma, J. Mater. Chem. 12 (2002) 1426–1436.
[3] R. Wang, J. Zhou, B. Li, L. Li, J. Alloys Compd. 490 (2010) 204–207.
[4] (a) S. Lysenko, J. Jimenez, V. Vikhnin, H. Liu, J. Lumin. 128 (2008) 821–823;
(b) R.P. Maiti, S. Basu, S. Bhattacharya, D. Chakravorty, J. Non-Cryst. Solids 355 (2009) 2254–2259.
[5] Z. Lin, X. Liang, Y. Ou, C. Fan, S. Yuan, H. Zeng, G. Chen, J. Alloys Compd. 496 (2010) L33–L37.
[6] T. Satyanarayana, I.V. Kityk, Y. Gandhi, V. Ravikumar, W. Kuznik, M. Piasecki, M.A. Valente, N. Veeraiah, J. Alloys Compd. 500 (2010) 9–15.
[7] S.A.M.A. Hameed, A.M. Fathi, J. Alloys Compd. 498 (2010) 71–76.
[8] (a) S. Duhana, N. Kishore, P. Aghamkarc, S. Devi, J. Alloys Compd. 507 (2010) 101–104;
(b) D. Xiong, J. Cheng, H. Li, J. Alloys Compd. 498 (2010) 162–167.
[9] E. Culea, L. Pop, M. Bosca, J. Alloys Compd. 505 (2010) 754–757.
[10] M. Wasiucionek, M. Foltyn, J.E. Garbarczyk, J.L. Nowinski, S. Gierlotka, B. Palosz, Solid State Ionics 179 (2008) 1278–1281.
[11] (a) A. Ghosh, S. Bhattacharya, A. Ghosh, J. Alloys Compd. 490 (2010) 480–483;
(b) S. Bhattacharya, A. Ghosh, Phys. Rev. B 68 (2003) 224202;
(c) A. Ghosh, J. Appl. Phys. 65 (1989) 227–230.
[12] H.I. Hsiang, L.T. Mei, C.S. Hsi, W.C. Liao, F.S. Yen, J. Alloys Compd. 502 (2010) 387–391.
[13] J.E. Garbarczyk, P. Jozwiak, M. Wasiucionek, J.L. Nowinski, Solid State Ionics 177 (2006) 2585–2588.
[14] J.S. Moya, S. Lopez-Esteban, C. Pecharroman, Prog. Mater. Sci. 52 (2007) 1017–1090.
[15] T.K. Pietrzak, J.E. Garbarczyk, I. Gorzkowska, M. Wasiucionek, J.L. Nowinski, S. Gierlotka, P. Jozwiak, J. Power Sources 194 (2009) 73–80.
[16] S. Radaa, M. Culea, M. Rada, T. Rusu, E. Culea, J. Alloys Compd. 490 (2010) 270–276.
[17] (a) M. Nagarjuna, T. Satyanarayana, Y. Gandhi, N. Veeraiah, J. Alloys Compd. 479 (2009) 549–556;
(b) P. Pascuta, G. Borodi, N. Jumate, I.V. Simiti, D. Viorel, E. Culea, J. Alloys Compd. 504 (2010) 479–483.
[18] (a) Y.B. Saddeek, K.A. Aly, A. Dahshan, I.M.El. Kashef, J. Alloys Compd. 494 (2010) 210–213;
(b) S.M. Salem, J. Alloys Compd. 503 (2010) 242–247.
[19] G. Lakshminarayana, J. Qiu, J. Alloys Compd. 478 (2009) 630–635.
[20] (a) S. Bhattacharya, A. Ghosh, Appl. Phys. Lett. 88 (2006) 133122;
(b) S. Bhattacharya, A. Ghosh, J. Phys. Chem. C 114 (2010) 5745–5750.
[21] N. Kuwata, T. Saito, M. Tatsumisago, T. Minami, J. Kawamura, J. Non-Cryst. Solids 324 (2003) 79–91.
[22] S.H. Santagneli, C.C. de Araujo, W. Strojek, H. Eckert, G. Poirier, S.J.L. Ribeiro, Y. Messaddeq, J. Phys. Chem. B 111 (2007) 10109–10117.
[23] (a) D. Dutta, A. Ghosh, J. Chem. Phys. 127 (2007) 044708;
(b) A. Pan, A. Ghosh, Phys. Rev. B 62 (2000) 3190–3195;
(c) A. Pan, A. Ghosh, J. Mater. Res. 17 (2002) 1941–1944.
[24] ICDD PDF-2 (release 2005), Card No. [00-021-1340], [00-075-1505] and [00-024-0715].
[25] B.D. Cullity, Elements of X-Ray Diffraction, Addison-Wesley, New York, 1956.
[26] T. Gloriant, M. Gich, S. Surinach, M.D. Baró, A.L. Greer, J. Met. Nanocryst. Mater. 8 (2000) 365–370.
[27] J. Soderlund, L.B. Kiss, G.A. Niklasson, C.G. Granqvist, Phys. Rev. Lett. 80 (1998) 2386–2388.
[28] T. Minami, T. Katsuda, M. Tanaka, J. Non-Cryst. Solids 29 (1978) 389–395.
[29] P. Znasik, M. Jamnicky, J. Non-Cryst. Solids 146 (1992) 74–80.
[30] M. Milanova, R. Iordanova, K.L. Kostov, J. Non-Cryst. Solids 355 (2009) 379–385.
[31] N. Machida, H. Eckert, Solid State Ionics 107 (1998) 255–268.